Highly Cooperative Valence Detrapping of Mixed-Valence $[Mn_3O(O_2CCH_3)_6(py)_3](py)$ in the Solid State

Ho G. Jang,[1a] John B. Vincent,[2a] Motohiro Nakano,[3] John C. Huffman,[2b] George Christou,*[,2a] Michio Sorai,*[,3] Richard J. Wittebort,*[,4] and David N. Hendrickson*[,1b]

Contribution from the Department of Chemistry, D-006, University of California at San Diego, La Jolla, California 92093-0506, School of Chemical Sciences, University of Illinois, Urbana, Illinois 61801, Department of Chemistry and the Molecular Structure Center, Indiana University, Bloomington, Indiana 47405, Department of Chemistry, University of Louisville, Louisville, Kentucky, 40292, and Chemical Thermodynamics Laboratory, Faculty of Science, Osaka University, Toyonaka, Osaka 560, Japan. *Received December 19, 1988*

Abstract: Heat capacity at constant pressure versus temperature data for $[Mn_3O(O_2CCH_3)_6(py)_3](py)$ show that there is a first-order phase transition at 184.65 K. The phase transition is characterized by total enthalpy and entropy gains of ΔH = 6460 J mol^{-1} and ΔS = 35.77 J K^{-1} mol^{-1}, respectively. The experimental ΔS is approximately equal to R ln 72 and is accounted for by two contributions: the Mn_3O complexes converting from valence trapped to valence detrapped (R ln 4) and the pyridine solvate molecules converting from being static to dynamically gaining access to 18 different orientations (R ln 18). The 18 different solvate molecule orientations result from the plane of each pyridine solvate jumping between three positions about the C_3 crystal axis, together with a rotation in each position about a local pseudo C_6 axis. To account for the ^{2}H NMR results the average orientation of the plane of the pyridine is not along the C_3 axis, but tipped off of it by ~15°. Variable-temperature ^{2}H NMR for a single crystal of $[Mn_3O(O_2CCD_3)_6(py)_3](py)$ oriented with the magnetic field parallel to the c axis establishes that there is an abrupt valence detrapping at the phase transition. Detailed ^{2}H NMR experimentation employing a new selective irradiation technique on a single crystal of $[Mn_3O(O_2CCH_3)_6(C_5D_5N)_3](C_5D_5N)$ verifies the onset and mechanism of motion of the pyridine solvate molecule at the phase transition. An explanation is given as to why the present Mn_3O complex exhibits valence detrapping abruptly in a first-order phase transition, whereas the isostructural Fe_3O complex valence detraps gradually in a higher order phase transition.

The rate of electron transfer in chemical and biological systems can be sensitively controlled by subtle environmental conditions.[5] Understanding how the specificity of electron flow is controlled in biological electron-transport chains is important.[6] The "docking" of two proteins could, for example, lead to a conformation change in one or both proteins and this could lead to an amino acid residue and/or the water structure about the redox center in one protein becoming dynamic. The onset of such dynamics could be a trigger, turning on the electron transfer into or out of that protein redox site. A polynuclear metal redox site having low-lying excited states, such as could be present in $[Fe_4S_4(SR)_4]^{3-}$ moieties,[7] may be switched on or off for electron transfer by the onset of environmental dynamics. This sensitivity is the result of vibronic interactions.[8]

The study of intramolecular electron-transfer events in mixed-valence metal complexes[9] in the solid state has given fundamental information about environmental effects on rates of electron transfer. Mixed-valence complexes are electronically labile. The lowest energy electronic states are vibronic and as a result the complexes are very sensitive to their environments. Simply changing the solvate molecule S in mixed-valence $[Fe_3O(O_2CCH_3)_6(L)_3]\cdot S$, where L is a ligand such as H_2O or pyridine(py), has been shown[10] to affect dramatically the rate of intramolecular electron transfer in the $Fe_2^{III}Fe^{II}O$ complex. Since it has been established[11] for several of these complexes that the valence detrapping (i.e., rapid electron transfer) occurs in a phase transition that also involves the cooperative onset of ligand and/or solvate molecule dynamics, there are basically two ways in which the solvate molecules can influence the rate of electron transfer. First, the presence of solvate molecules can affect the magnitude of intermolecular interactions between Fe_3O complexes. Appreciable intermolecular interactions will trap the valences in a Fe_3O complex. Second, van der Waals interactions between S and Fe_3O molecules could lead to an environment about a Fe_3O complex of symmetry lower than C_3. The ground-state potential energy surface for each Fe_3O complex is changed by such van der Waals interactions. Slow rates of electron and/or nuclear tunneling develop in the Fe_3O complex for low-symmetry environments provided by the S solvate molecules. If the solvate molecules experience the onset of dynamics in a phase transition, this would likely tend to symmetrize the environment about neighboring Fe_3O complexes and consequently increase the rate of tunneling in the complex.

(1) (a) University of Illinois. (b) University of California at San Diego.
(2) (a) Indiana University, Department of Chemistry. (b) Indiana University, Molecular Structure Center.
(3) Osaka University.
(4) University of Louisville.
(5) (a) Cannon, R. D. *Electron Transfer Reactions*; Buttersworth: Boston, MA, 1980. (b) Mikkelsen, K. V.; Ratner, M. A. *Chem. Rev.* **1987**, *87*, 113. (c) Marcus, R. A.; Sutin, N. *Biochim. Biophys. Acta* **1985**, *811*, 265.
(6) (a) DeVault, D. *Quantum-Mechanical Tunnelling in Biological Systems*, 2nd ed.; Cambridge University Press: Cambridge, England, 1984. (b) Jortner, J. *Biochim. Biophys. Acta* **1980**, *594*, 193. (c) Williams, G.; Moore, G. R.; Williams, R. J. P. *Comments Inorg. Chem.* **1985**, *4*, 55. (d) Williams, R. J. P.; Concar, D. *Nature* **1986**, *322*, 213. (e) Dixit, B. P. S. N.; Vanderkooi, J. M. *Curr. Top. Bioenerg.* **1984**, *13*, 159.
(7) Carney, M. J.; Papaefthymiou, G. C.; Spartalina, K.; Frankel, R. B.; Holm, R. H. *J. Am. Chem. Soc.* **1988**, *110*, 6084.
(8) (a) Bersuker, I. B. *The Jahn-Teller Effect and Vibronic Interactions in Modern Chemistry*; Plenum Press: New York, 1984. (b) Wong, K. Y.; Schatz, P. N. *Prog. Inorg. Chem.* **1981**, *28*, 369.
(9) For recent reviews, see: (a) Day, P. *Int. Rev. Phys. Chem.* **1981**, *1*, 149. (b) *Mixed-Valence Compounds, Theory and Applications in Chemistry, Physics, Geology, and Biology*; Brown, D. B., Ed.; Reidel: Boston, MA, 1980. (c) Creutz, C. *Prog. Inorg. Chem.* **1983**, *30*, 1-73. (d) Richardson, D. E.; Taube, H. *Coord. Chem. Rev.* **1984**, *60*, 107.
(10) (a) Oh, S. M.; Hendrickson, D. N.; Hassett, K. L.; Davis, R. E. *J. Am. Chem. Soc.* **1984**, *106*, 7984. (b) Oh, S. M.; Hendrickson, D. N.; Hassett, K. L.; Davis, R. E. *J. Am. Chem. Soc.* **1985**, *107*, 8009.
(11) (a) Oh, S. M.; Kambara, T.; Hendrickson, D. N.; Sorai, M.; Kaji, K.; Woehler, S. E.; Wittebort, R. J. *J. Am Chem. Soc.* **1985**, *107*, 5540. (b) Sorai, M.; Kaji, K.; Hendrickson, D. N.; Oh, S. M. *J. Am. Chem. Soc.* **1986**, *108*, 702. (c) Woehler, S. E.; Wittebort, R. J.; Oh, S. M.; Hendrickson, D. N.; Inniss, D.; Strouse, C. E. *J. Am. Chem. Soc.* **1986**, *108*, 2938. (d) Woehler, S. E.; Wittebort, R. J.; Oh, S. M.; Kambara, T.; Hendrickson, D. N.; Inniss, D.; Strouse, C. E. *J. Am. Chem. Soc.* **1987**, *109*, 1063. (e) Oh, S. M.; Wilson, S. R.; Hendrickson, D. N.; Woehler, S. E.; Wittebort, R. J.; Inniss, D.; Strouse, C. E. *J. Am. Chem. Soc.* **1987**, *109*, 1073. (f) Hendrickson, D. N.; Oh, S. M.; Dong, T.-Y.; Kambara, T.; Cohn, M. J.; Moore, M. F. *Comments Inorg. Chem.* **1985**, *4*, 329. (g) Sorai, M.; Shiomi, Y.; Hendrickson, D. N.; Oh, S. M.; Kambara, T. *Inorg. Chem.* **1987**, *26*, 223.

0002-7863/89/1511-7778$01.50/0

Of the mixed-valence Fe_3O acetate complexes, $[Fe_3O(O_2CCH_3)_6](py)$ (**1**) is the most studied.[10a,10b,11b,11d] Heat capacity measurements show that this compound has a first-order phase transition at ~112 K with a higher order phase transition starting at ~115 K and culminating at ~190 K. The 115–190 K higher order phase transition has been shown by variable-temperature ^{57}Fe Mössbauer and solid-state ^2H NMR results to involve both the onset of rapid electron transfer in the Fe_3O complexes and the onset of dynamics associated with the pyridine solvate molecules. In the latter case the plane of each pyridine solvate molecule jumps between three positions along the crystallographic C_3 axis, which appears above ~190 K.

Preliminary work[12] indicated the onset of valence detrapping for $[Mn_3O(O_2CCH_3)_6(py)_3](py)$ (**2**) is quite different from that observed for $[Fe_3O(O_2CCH_3)_6(py)_3](py)$ (**1**), even though both compounds are isostructural. It is shown in the present paper that, in contrast to the situation for the analogous Fe_3O complex **1**, the onset of rapid electron transfer for complex **2** occurs abruptly in a first-order phase transition. An explanation is advanced for why there is so much more cooperativity in the valence detrapping of Mn_3O complex **2** than for the Fe_3O complex **1**.

Experimental Section

Compound Preparation. The deuterated chemicals, pyridine-d_5 (99.5% D) and acetic acid-d_4 (99% D), were purchased from Aldrich Chemical Co. and were used without further purification. All elemental analyses were performed in the Microanalytical Laboratory of the School of Chemical Sciences, University of Illinois. Purified solvents and dried compounds were always stored and manipulated under an argon atmosphere.

Samples of $[Mn_3O(O_2CCH_3)_6(py)_3](py)$ (**2**) were prepared as previously described.[12] A 2.00-g (8.15 mmol) sample of $Mn(O_2CCH_3)_2{\cdot}4H_2O$ was dissolved in a mixture of glacial acetic acid (10 mL) and pyridine (20 mL). The resulting solution was stirred while 0.76 g (2.1 mmol) of $(n\text{-}Bu)_4NMnO_4$ was added in small portions to yield a dark brown/black homogeneous solution. The solution was then slowly evaporated for 2 days and the precipitate collected by filtration and dried under vacuum. The yield was ~65%. Anal. Calcd for $C_{32}H_{38}N_4O_{13}Mn_3$: C, 45.13; H, 4.47; N, 6.58; Mn, 19.37. Found: C, 44.96; H, 4.48; N, 6.42; Mn, 19.54. Crystalline samples of $[Mn_3O(O_2CCD_3)_6(py)_3](py)$ and $[Mn_3O(O_2CCH_3)_6(C_5D_5N)_3](C_5D_5N)$ were prepared by the same method employing deuterated reagents.

Heat Capacity Measurements. Heat capacities were measured with an adiabatic calorimeter[13] between 13 and 300 K. A calorimeter cell[14] made of gold-plated copper was loaded with 16.4551 g of $[Mn_3O(O_2CCH_3)_6(py)_3](py)$, with buoyancy correction in which the density of the same was taken as 1.456 g cm^{-3}. A small amount of helium gas was sealed in the cell to aid in heat transfer. Considerable details of the heat capacity data collection and analysis for $[Mn_3O(O_2CCH_3)_6(py)_3](py)$ are available in another paper.[15]

Solid-State ^2H NMR Spectroscopy. ^2H NMR spectra were obtained on a "home-built" 5.9-T spectrometer described previously.[16] For all experiments except those using selective excitation a standard pulse sequence of $(90)_x - t - (90)_y - t -$ observe was used with t = 30–50 μs and a 90° pulse width of 2.7 μs. Selective excitation experiments for identifying quadrupolar coupled doublets used the sequence $(180)_{sel}$: $(90)_x - t - (180)_y - t - (90)_y - t - (180)_y - t -$ observe, with t = 25 μs. On alternate shots, the selective irradiation pulse, $(180)_{sel}$, was turned off and the resulting signal subtracted from memory, leading to cancellation of all peaks except those at the irradiation frequency or those quadrupole coupled to the irradiated peak.[17] The 90° pulse widths for the selective and nonselective pulses were 50 and 2.5 μs, respectively. In the case of the magnetically oriented microcrystalline sample, ~40 mg of complex **2** and degassed hexadecane (mp 18 °C) were sealed in a Delrin tube ($^1/_4 \times {}^1/_2$ in.). The tube was then introduced into the 5.9-T magnetic field where the microcrystals were oriented such that the principal axis (C_3 crystal axis) of the magnetic susceptibility tensor of each crystal was aligned with the magnetic field. The hydrocarbon matrix was then cooled in the magnetic field to temperatures below the 18 °C melting point to form a solid block with the crystals embedded in it.

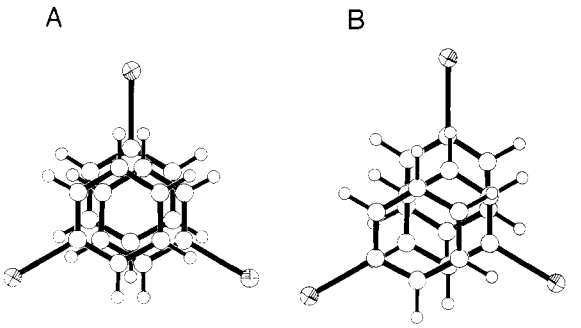

Figure 1. ORTEP view along c axis of intermolecular pyridine–pyridine overlaps in (A) $[Mn_3O(O_2CCH_3)_6(py)_3](py)$ and (B) $[Fe_3O(O_2CCH_3)_6(py)_3](py)$. In the case of each pyridine ligand the metal atom to which it is bonded is also shown.

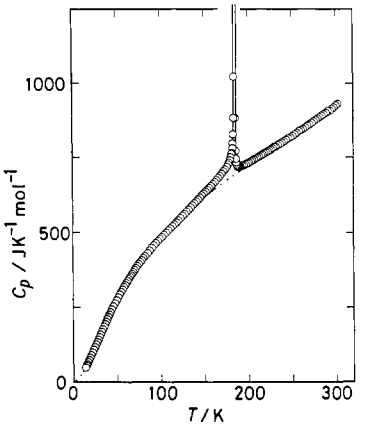

Figure 2. Heat capacity at constant pressure, C_P, versus temperature for a 16.4551-g sample of $[Mn_3O(O_2CCH_3)_6(py)_3](py)$.

Results and Discussion

Solid-State Structure of $[Mn_3O(O_2CCH_3)_6(py)_3](py)$. Previously we reported[12] the −50 °C X-ray structure of complex **2**. This complex crystallizes in rhombohedral space group $R32$. Mn_3 is an equilateral triangle. Along the c axis Mn_3O complexes and pyridine solvate molecules are stacked, occupying alternating sites of 32 symmetry. Each stack is surrounded by three other stacks. There is an appreciable py···py overlap between the pyridine ligands of one Mn_3O complex and those of nearby complexes. The stacking c axis (10.918 Å) in Mn_3O complex **2** is 0.065 Å larger than in the isostructural Fe_3O complex **1**. However, even though the c axis is larger in the Mn_3O than in the Fe_3O complex, there is probably a greater interaction in the Mn_3O case. As can be seen in Figure 1, the intermolecular py···py contact is nearly eclipsed for the Mn_3O complex **2**, whereas for Fe_3O complex **1** the intermolecular py···py contact is appreciably slipped.

In our previous[12] examination of the structure of complex **2** we concluded from a difference Fourier map that the pyridine solvate molecule is lying on and seriously disordered about the crystallographic C_3 axis. In view of the solid-state ^2H NMR and heat capacity results presented in this paper, we took a closer look at this pyridine solvate molecule. It is difficult to present a definitive picture of the disorder of the pyridine solvate molecule. A careful reexamination of the difference Fourier map indicates that the plane of the pyridine solvate molecule lies off the C_3 axis, contrary to our previous assessment. Obviously, the pyridine solvate molecule is disordered as well about the crystallographic C_3 axis.

Heat Capacity of $[Mn_3O(O_2CCH_3)_6(py)_3](py)$ (2). The heat capacity under constant pressure, C_P, was measured for a 16.4551-g sample of complex **2** in the range of 13–300 K. As detailed in another paper,[15] it was particularly important that the crystalline sample used in these measurements was freshly re-

(12) Vincent, J. B.; Chang, H.-R.; Folting, K.; Huffman, J. C.; Christou, G.; Hendrickson, D. N. *J. Am. Chem. Soc.* **1987**, *109*, 5703.
(13) Sorai, M.; Kaji, K., unpublished results.
(14) Ogasahara, K.; Sorai, M.; Suga, H. *Mol. Cryst. Liq. Cryst.* **1980**, *71*, 189.
(15) Nakano, M.; Sorai, M.; Vincent, J. B.; Christou, G.; Jang, H. G.; Hendrickson, D. N. *Inorg. Chem.*, in press.
(16) Wittebort, R. J.; Subramanian, R.; Kulshreshtha, N. P.; DuPre, D. B. *J. Chem. Phys.* **1985**, *83*, 2457.
(17) Wittebort, R. J. *J. Magn. Reson.*, in press.

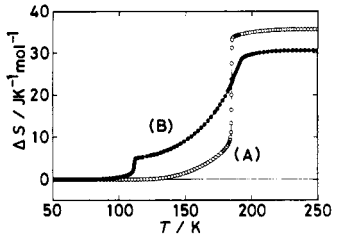

Figure 3. Plot of entropy gain, ΔS, versus temperature for (A) $[Mn_3O(O_2CCH_3)_6(py)_3](py)$ and (B) $[Fe_3O(O_2CCH_3)_6(py)_3](py)$.

crystallized and had a full 1.00 mol of solvate pyridine. Samples with less than 1.00 mol of solvate pyridine were found to exhibit more than one C_P peak. In Figure 2 is given a plot of C_P versus temperature for the freshly recrystallized sample of complex **2**. A single very sharp peak arising from a phase transition is observed at 184.65 K. The maximum of C_P at the 184.65 K peak approaches 12 000 J K^{-1} mol^{-1}. This phase transition clearly is of first order, as indicated by the sharpness of the heat capacity effect and by a long thermal relaxation time near T_C (~30 min time to reach thermal equilibrium after an electrical input to raise the temperature by only tenths of a degree near T_C).

A "normal" heat capacity curve was determined as a sum of two terms, a magnetic contribution and a contribution from intramolecular and lattice vibrations (ref 15 should be consulted for details). The magnetic contribution was evaluated from the magnetic exchange interaction parameters obtained in the magnetic susceptibility study[12] of complex **2**. The difference between the observed and "normal" heat capacities is the excess heat capacity, ΔC_P, due to the phase transition. Integration of ΔC_P with respect to ln T gives the transition entropy, ΔS. A plot of ΔS versus temperature for the Mn_3O complex **2** is shown in Figure 3. For comparison purposes, the ΔS versus temperature data previously reported[11b] for isostructural $[Fe_3O(O_2CCH_3)_6(py)_3](py)$ (**1**) are also plotted in Figure 3.

For Mn_3O complex **2** we calculate total changes of ΔS = 35.77 J K^{-1} mol^{-1} and ΔH = 6460 J mol^{-1}. As can be seen in Figure 3, approximately 24 J K^{-1} mol^{-1} of the total ΔS value occurs very abruptly near to the transition temperature. This 24 J K^{-1} mol^{-1} value agrees well with the value of ΔS = 24.7 J K^{-1} mol^{-1} obtained in the DSC experiment.[12] In view of the relatively fast scan rates used in recording DSC thermograms, it is understandable that the DSC experiment would only readily detect the abrupt ΔS contribution. Regardless, ~$^2/_3$ of the total ΔS for the single phase transition observed for the Mn_3O complex **2** occurs abruptly in a narrow temperature range. The other ~$^1/_3$ of the total ΔS is accumulated gradually in the ~140–182 K range.

The ΔS versus temperature characteristics for Fe_3O complex **1** stand in marked contrast to those of Mn_3O complex **2** (see Figure 3). The total ΔS for both phase transitions of the Fe_3O complex **1** was found[11b] to be 30.53 J K^{-1} mol^{-1}. As the sample temperature is increased from 13 K some 4.61 K^{-1} mol^{-1} is gained abruptly in the first-order phase transition at ~112 K. The remaining ΔS value of ~26.0 J K^{-1} mol^{-1} is gradually accumulated in the higher order phase transition, which starts at ~115 K and culminates at ~190 K. There is, thus, a very dramatic difference in the rate at which entropy is accumulated in what are valence-detrapping phase transitions in these isostructural Mn_3O and Fe_3O complexes. In a later section we will discuss the possible origin of this difference.

It is important to emphasize that from both the perspectives of single-crystal X-ray diffractometry and chemical analysis it is likely the crystallinity in the case of Fe_3O complex **1** is better than in the case of Mn_3O complex **2**. The Mn_3O complex more readily tends to lose pyridine solvate molecules, as clearly indicated by chemical analysis data. Furthermore, the X-ray diffraction quality of the Fe_3O complex is better than that of the Mn_3O complex. As a consequence, it does not seem possible to attribute the differences in ΔS versus temperature in the two complexes to a smearing out of a first-order phase transition in the Fe_3O complex as the result of a higher level of defect concentration.

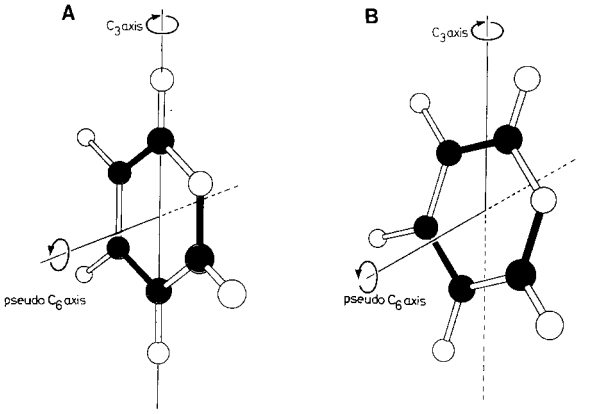

Figure 4. Views of two possible motions of the pyridine solvate molecules in the high-temperature phase of $[Mn_3O(O_2CCH_3)_6(py)_3](py)$. In both parts A and B, each pyridine solvate rotates about a local pseudo C_6 axis. In part A, the plane of pyridine solvate is along the C_3 axis. In part B, the plane of pyridine solvate is tipped ~15° off the C_3 axis.

After all, the Fe_3O complex does show a *sharp* C_P peak at ~112 K as well as the broad 115–190 K thermal effect.

The experimental value of ΔS = 35.77 J K^{-1} mol^{-1} for complex **2** is close to the value of $\Delta S = R$ ln 72 (=35.56 J K^{-1} mol^{-1}). This suggests an origin for the entropy gain. There are probably two contributions to the total ΔS for the phase transition. As demonstrated in the next section, the phase transition involves both the Mn_3O complexes going from valence trapped to valence detrapped and the pyridine solvate molecules changing from static at low temperature to dynamic at high temperature.

Evidence for the valence detrapping in the Mn_3O complex **2** comes from three experimental facts. First, the results of the 223 K X-ray structure show that the Mn_3O complexes have a 3-fold symmetry with all three Mn atoms being equivalent. Second, the 10-kG magnetic susceptibility results below the phase-transition temperature for complex **2** have been well accounted for in terms of the Heisenberg–Dirac–Van Vleck (HDVV) model, which is based on a valence-trapped state.[12] Third, the ^2H NMR results for a single crystal of $[Mn_3O(O_2CCD_3)_6(py)_3](py)$ show by virtue of the equivalence of the six deuteriomethyl groups that all three Mn atoms in the complex are equivalent (vide infra). In the phase transition the Mn_3O complex changes from being trapped in one vibronic state to interconverting rapidly between four vibronic states. This contributes $\Delta S = R$ ln 4 to the total transition entropy gain.

As is verified by the ^2H NMR results, the pyridine solvate molecules convert from a static situation at low temperatures to interconverting dynamically among distinguishable positions in the lattice above T_C = 184.65 K. As shown in Figure 4A, one way this could occur is by the plane of each pyridine solvate molecule jumping between three different positions as a result of dynamics about the crystallographic C_3 axis. There could be a second motion where each pyridine solvate also rotates about a local pseudo C_6 axis. In this way each pyridine solvate accesses 18 different orientations. This contributes $\Delta S = R$ ln 18 to the total transition entropy. Adding this to the R ln 4 contribution from valence detrapping the Mn_3O complex gives a total of $\Delta S = R$ ln 72 (=35.56 J K^{-1} mol^{-1}), which compares favorably to the experimental value of ΔS = 35.77 J K^{-1} mol^{-1}.

Solid-State ^2H NMR Spectroscopy. ^2H NMR experiments were carried out on two different deuterated forms of complex **2**: $[Mn_3O(O_2CCD_3)_6(py)_3](py)$ and $[Mn_3O(O_2CCH_3)_6(C_5D_5N)_3](C_5D_5N)$. There are two types of interactions apparent in a ^2H NMR spectrum of a paramagnetic compound. The nuclear quadrupole interaction of the ^2H (I = 1) nucleus gives rise to a doublet for each different deuteron site. In addition, there is a through-space dipolar interaction of the magnetic moment of the unpaired electrons of the Mn_3O complex with the nuclear magnetic moment of the ^2H nucleus. As a consequence, the quadrupole-split ^2H NMR doublet is shifted from the usual diamagnetic Larmor frequency (defined as zero) by this dipolar interaction, which varies

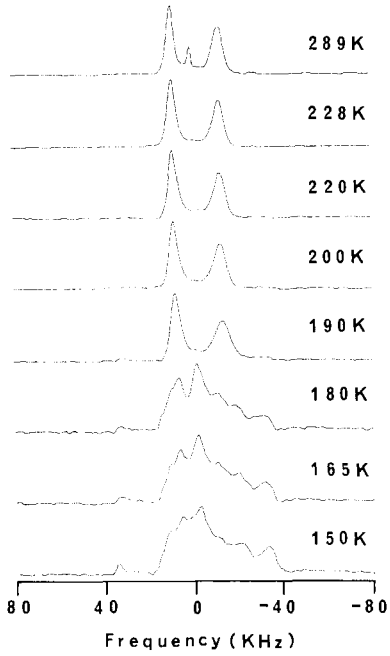

Figure 5. Variable-temperature ^2H NMR spectra for a $\sim 1.5 \times 1.5 \times 1.5$ mm single crystal of $[Mn_3O(O_2CCD_3)_6(py)_3](py)$ embedded in hexadecane and oriented so that the magnetic field is parallel to the crystallographic c axis.

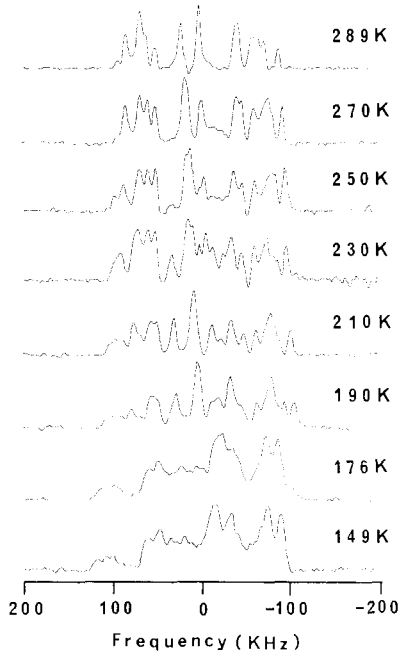

Figure 6. Variable-temperature ^2H NMR spectra for a $\sim 1.5 \times 1.5 \times 1.5$ mm single crystal of $[Mn_3O(O_2CCH_3)_6(C_5D_5N)_3](C_5D_5N)$ embedded in hexadecane and oriented so that the magnetic field is parallel to the crystallographic c axis.

inversely with the cube of the distance between the nuclear and electron spin moments. Further discussion of the theoretical factors affecting the ^2H NMR spectrum of a paramagnetic compound in the solid state are available.[11c,d,e]

Variable-temperature ^2H NMR experiments were carried out on a $\sim 1.5 \times 1.5 \times 1.5$ mm single crystal of $[Mn_3O(O_2CCD_3)_6(py)_3](py)$. In these experiments the CD_3 deuterons are used as a probe of whether the Mn_3O complex is valence trapped or detrapped on the time scale of the ^2H NMR technique. The single crystal, suspended at room temperature in liquid hexadecane (mp 18 °C), turns in the 5.9-T magnetic field until the largest component of the magnetic susceptibility tensor aligns along the magnetic field direction. The sample was then cooled, thus fixing the crystal in a known orientation relative to H_0. In Figure 5 are shown variable-temperature spectra taken with the magnetic field parallel to the principal axis of the susceptibility tensor of the crystal. In the temperature range of 190–289 K the spectrum shows a single quadrupole-split doublet, shifted somewhat from zero frequency. The presence of one doublet clearly indicates that all six CD_3 groups of each Mn_3O complex are equivalent in terms of dipolar and quadrupolar coupling interactions. This is only possible when the magnetic field is oriented along the crystallographic c axis (i.e., the easy axis) and when the Mn_3O complexes are interconverting between their four vibronic states rapidly on the ^2H NMR time scale. All three Mn ions are effectively equivalent.

In the solid state, the CD_3 groups of $[Mn_3O(O_2CCD_3)_6(py)_3](py)$ are likely rotating rapidly about their local C_3 axes at temperatures below even 100 K. For such a rapidly rotating CD_3 group, the motionally averaged residual quadrupole splitting tensor has components of $\langle V_{zz} \rangle = 42$ kHz, $\langle V_{xx} \rangle = \langle V_{yy} \rangle = -21$ kHz, assuming that the quadrupole coupling constant for a static CD_3 group is 165 kHz.[18] Thus, when the magnetic field is directed perpendicular to the local C_3 axis of the rapidly rotating CD_3 group, the observed quadrupole splitting is expected to be 42 kHz. However, Figure 5 shows that in the 190–287 K range the quadrupole splitting is observed to be 22.4 kHz $[= (\nu_1 - \nu_2)]$. This means that the angle between the magnetic field and the principal component of the CD_3 residual quadrupole tensor is calculated to be ~45°. From the 223 K X-ray structure[12] the angle between the local C_3 axis of the CD_3 group and the crystallographic c axis is ~45°. It is clear that this crystal aligns with its c axis along the magnetic field and $[Mn_3O(O_2CCD_3)_6(py)_3](py)$ is valence detrapped above ~190 K on the ^2H NMR time scale.

As can be seen in Figure 5 the ^2H NMR spectrum for a crystal of $[Mn_3O(O_2CCD_3)_6(py)_3](py)$ changes abruptly from a spectrum with one doublet above ~190 K to a poorly resolved spectrum with many doublets below ~180 K. This is clear and dramatic evidence that the phase transition in the 180–190 K region involves a conversion from valence trapped to valence detrapped. This agrees with the C_P data, which show a phase transition at 184.65 K.

The appearance of from four to six doublets in the 150 K CD_3 spectrum (Figure 5) also was observed[12] for $[Fe_3O(O_2CCD_3)_6(py)_3](py)$ at low temperatures. Several doublets can be seen, not just two doublets as simply expected for a $Mn_2^{III}Mn^{II}$ valence-trapped complex. Valence trapping could distort the Mn_3O complex. Also, it is important to note that each CD_3 moiety experiences dipolar interactions not only with the unpaired electrons in its own molecule, but the CD_3 moieties are as close in the solid state to neighboring Mn_3O complexes. The low-temperature CD_3 spectra for the Mn_3O and Fe_3O complexes are, however, appreciably different in detail. The peaks in the Mn_3O spectrum (Figure 5) are broader and encompass a larger magnetic field range than those in the Fe_3O spectrum.[11d] This likely reflects the fact that, since the antiferromagnetic pairwise exchange interactions are weaker in the Mn_3O complex than in the Fe_3O complex,[12] there are more spin states populated for the Mn_3O complex in the 150–170 K range and more effective spin–lattice relaxation. The larger value of μ_{eff} of the Mn_3O complex in this range leads also to larger dipolar shifts as observed.

In Figure 6 is shown the temperature dependence of the ^2H NMR spectrum of a $\sim 1.5 \times 1.5 \times 1.5$ mm crystal of $[Mn_3O(O_2CCH_3)_6(C_5D_5N)_3](C_5D_5N)$ oriented in wax so that the magnetic field is parallel to the crystallographic c axis. It is important to describe the order in which these spectra were recorded. First, the 298 K spectrum was run and then the sample was cooled to 270 K and equilibrated for ~30 min before the 270 K spectrum was recorded. The crystal was then cooled to 149 K and after 4–5 h a spectrum was recorded at 149 K. The sample temperature was then increased to 176, 190, 210, 230, and 250 K, and in each step the sample was equilibrated for ~20–30 min

(18) (a) Seelig, J. *Q. Rev. Biophys.* **1977**, *10*, 353. (b) Barnes, R. G. *Advances in Nuclear Quadrupole Resonance*; Smith, A. J. S., Ed.; Heyden: London, 1972; Vol. 1.

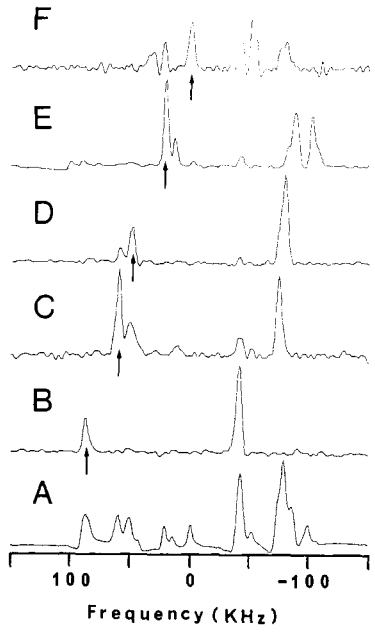

Figure 7. ^2H NMR spectra obtained for a single crystal of $[Mn_3O(O_2CCH_3)_6(C_5D_5N)_3](C_5D_5N)$ embedded in a hexadecane matrix and oriented with the magnetic field parallel to the c axis of the crystal. Spectrum A was obtained with a single nonselective pulse train. Spectra B–F were obtained as difference signals resulting from a selective pulse train with frequency centered at the position of the arrow.

before a spectrum was recorded. Crystals of this compound do survive cycling through the phase transition. Three initial observations can be made about the temperature dependence of these spectra. First, the 250 K spectrum obtained upon heating the sample looks very similar to the 270 K spectrum obtained when first cooling the sample. Second, there is a fairly dramatic change in the spectrum upon heating the sample from 176 to 190 K, reflecting the phase transition at 184.65 K. The general trend is equivalent to that observed in Figure 5. As the temperature is lowered below 190 K, the loss of resolution is likely due to both a substantial increase in the number and width of the lines. Third, several peaks seem to be shifting to some degree in the 190–250 K region.

Since the heat capacity results show that the phase transition for this Mn_3O complex is first order, one could anticipate that not nearly enough time was spent equilibrating the crystal at the various temperatures. In fact, it is quite possible that equilibrium was not fully established in the cycle 176, 190, 210, 230, and then 250 K. Thus, perhaps the full dynamics of the pyridine solvate molecules are only slowly being established in the 190–250 K range. With the experimental setup we employed it was just not possible to keep the single-crystal sample cooled at low temperatures for longer periods of time. Also, it was not deemed necessary to do so, for the goal was 2-fold: (1) find out if the pyridine solvate molecule experiences an onset of motion at the 184.65 K phase transition; and (2) discover the mechanism of pyridine solvate molecule motion. From Figure 6, it is clear that there is some change in dynamics at the phase transition.

In recent work[17] we demonstrated an attractive way to pick out pairs of quadrupole-coupled peaks in complicated ^2H NMR spectra such as these. In this experiment, a single line in the spectrum is selectively irradiated. In effect, the presence of the quadrupole coupling leads to a magnetization transfer between the irradiated peak and its quadrupole-coupled pair. The entire spectrum is then nonselectively excited, and with the use of difference techniques, only the selectively excited peak and its quadrupole-coupled pair(s) are observed. Figure 7 illustrates the results obtained employing the technique with a single crystal of $[Mn_3O(O_2CCH_3)_6(C_5D_5N)_3](C_5D_5N)$ oriented with the magnetic field along the c axis at 275 K. Plot A gives the usual spectrum obtained with nonselective excitation. All peaks are seen. Spectrum B shows the difference signal resulting from selective irradiation centered at the position of the arrow. Two peaks are seen, the one where the selective pulse train was centered (88 kHz) and another at −43 kHz. These two peaks comprise one quadrupole-split doublet with a splitting of 131 kHz. This quadrupole splitting is that expected[18b] for a static pyridine ring deuteron with the C–D vector perpendicular to H_0. This 88/−43 kHz doublet is dipolar shifted 22 kHz to low field.

For spectrum C the selective pulse was centered at 60.4 kHz. The other peak with appreciable intensity is seen at −76 kHz. This pair is assignable as another static pyridine ligand doublet. In spectra A and C it can be seen that, in addition to the 60.4/−76 kHz doublet, there is at least one other doublet that is quite close to this one. In spectrum D is shown the result of selective irradiation at 51.3 kHz, where a peak at −80 kHz is identified. Thus, there are two nearby doublets with quadrupole splittings of ~130–135 kHz and dipolar shifted by 8–14 kHz to high field. These doublets are clearly associated with static deuteron sites of pyridine ligands.

In the case of spectrum E the selective pulse occurred at 21 kHz. In addition to the nearby 14.5 kHz resonance, which is only partially excited, peaks are seen at ~−88 and ~−99 kHz. Thus, there also seems to be at least two "static-deuteron" doublets in this spectral region, dipolar shifted to high field by ~38 kHz. Without full rotational studies of these different doublets it is difficult to assign them. It is possible that the doublet identified in spectrum B is for the para deuterons on the pyridine ligands. The two doublets detected in spectra C and D could be assigned to the meta deuterons, and finally, the two doublets in evidence in spectrum E could be for the ortho deuterons. With each Mn_3O complex having 32-site symmetry, only one doublet for the meta deuterons and one doublet for the pyridine ligand ortho deuterons are expected. It is suggested that the X-ray structure only shows a spatial average and that there are really present in the crystal slightly different positions for the pyridine ligands twisted from being perpendicular to the C_3 axis. Other possibilities are that there are twinned domains in the single crystal where the C_3 axes are slightly misaligned or that the magnetic alignment is not perfect.

Examination of the full spectrum in trace A shows that there is only one remaining low-field peak that could be associated with the pyridine solvate deuterons. From the heat capacity data it is expected that at 275 K the pyridine solvate molecules are involved in some dynamical motion, which would reduce the quadrupole splitting from the 264 kHz static value.[19] In spectrum F is shown the outcome when the selective pulse is centered at the 0.1-kHz peak. For peaks near the center of the spectrum the selectivity is not expected to be good.[17] The only peak that is enhanced which was not previously accounted for is −52 kHz. It is concluded that the five deuterons associated with the pyridine solvate molecule give one doublet with peaks at 0.1 and −52 kHz, i.e., have quadrupole coupling and paramagnetic shifts of 26 and −26 kHz, respectively.

A simple way to get one doublet for all five pyridine solvate deuterons is for there to be fast rotation of each pyridine solvate molecule about a local pseudo C_6 axis as illustrated in Figure 4A. This was also surmised from the heat capacity data. A model to explain the observed $\langle V_{zz} \rangle$ = 26 kHz for the single solvate doublet is as follows. If, in addition to the fast in-plane C_6 rotation of each solvate, the plane of each pyridine solvate jumps between three positions distributed about the crystallographic C_3 axis, then the observed $\langle V_{zz} \rangle$ value can be rationalized. One small adjustment is needed. According to the quadrupolar coupling tensor matrix, the angle (α) between the external magnetic field (collinear with the C_3 axis) and the average C–D vector of pyridine solvate deuterons can be calculated to be $\alpha \cong 75°$ at 298 K. In each of the three positions about the C_3 axis the pyridine plane is tipped ~15° off the C_3 axis. Thus, each pyridine jumps between three

(19) Barnes, R. G.; Bloom, J. W. *J. Chem. Phys.* **1972**, *57*, 3082.
(20) Wittebort, R. J.; Olejniczak, E. T.; Griffin, R. G. *J. Chem. Phys.* **1987**, *86*, 5411.

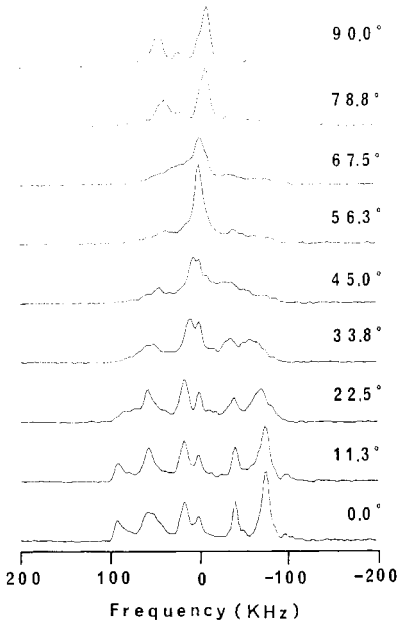

Figure 8. ^2H NMR spectra for magnetically oriented microcrystalline sample of $[Mn_3O(O_2CCH_3)_6(C_5D_5N)_3](C_5D_5N)$ embedded in an eicosane matrix at 275 K. The angle between the magnetic field and the principal axis of the susceptibility tensor (i.e., *c* axis) is given for each spectrum.

positions on a cone $\sim 15°$ off the C_3 axis and also rapidly rotates about a C_6 axis in each position, as shown in Figure 4B. This model is not only consistent with the heat capacity and ^2H NMR results but also agrees with the X-ray crystallography, which suggests the pyridine planes are tipped off the C_3 axis. Since the *c* axis for $[Mn_3O(O_2CCH_3)_6(py)_3](py)$ is 0.065 Å larger than in $[Fe_3O(O_2CCH_3)_6(py)_3](py)$, it is reasonable that the pyridine solvate molecule rattles around more in the cavity of the Mn_3O lattice than in the Fe_3O lattice.

The proposed 3-fold motion about the *c* axis would render the quadrupole and paramagnetic coupling tensors axially symmetric about this axis. Thus, if a magnetically oriented microcrystalline sample, which is ordered about this axis but disordered in the plane perpendicular, is fixed in wax and rotated off the magnetic field, the solvate NMR line should remain well-resolved. The ligand deuterons, with quadrupole couplings randomly oriented in the plane of disorder thus contribute to a pattern that becomes increasingly broad as the rotation angle approaches 90°. At the 90° orientation, the solvate should show a resolved doublet at 26 and 0 kHz, based on the data from above. This procedure is shown in Figure 8, and although there is considerable spectral overlap, the expected peak at 26 kHz in the 90° spectrum is clearly observed.

^{57}Fe Mössbauer Data. An attempt was made to dope a small amount (2 mg) of 100% ^{57}Fe-enriched Fe_3O complex into 200 mg of $[Mn_3O(O_2CCH_3)_6(py)_3](py)$. The two microcrystalline solids were dissolved together in purified pyridine in an argon-charged glovebox. Partial evaporation gave ~ 80 mg of a microcrystalline solid. After the fact it was not too surprising to find that in solution there was a redox reaction where all the Fe^{II} in the Fe_3O complex was oxidized by Mn_3O complexes. Mössbauer spectra run from 110 to 300 K showed only one doublet for a high-spin Fe^{III} ion. Thus, the solid contains a small amount of $[Fe_2^{III}Mn^{II}O(O_2CCH_3)_6(py)_3](py)$ doped into $[Mn_3O(O_2CCH_3)_6(py)_3](py)$. It was *not* possible to study the onset of valence detrapping in a $Fe_2^{III}Fe^{II}O$ dopant occurring when the whole Mn_3O lattice detrapped at the phase transition. However, we could study the temperature dependence of the recoilless fraction for the $Fe_2^{III}Mn^{II}$ dopant sites. Figure 9 gives a plot of minus the natural logarithm of the base-line-normalized spectral areas versus temperature for this doped sample. One straight line is expected for a lattice that is not changing its vibrational nature throughout the temperature region. As can be seen in Figure 9, there is a change from one straight line to another occurring at the phase transition. There is a change in the vibrational nature of the solid at ~ 184 K.

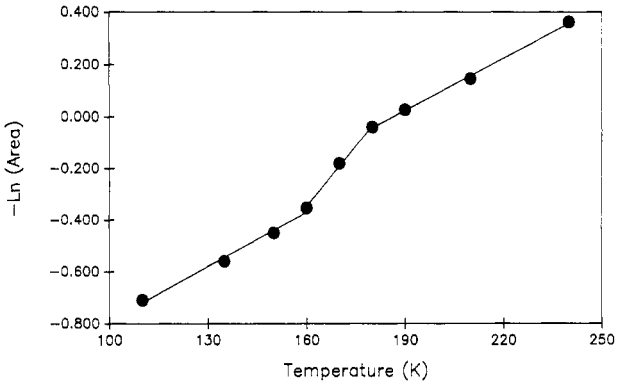

Figure 9. Plot of minus the natural logarithm of the base-line-normalized spectral areas versus temperature evaluated from the ^{57}Fe Mössbauer spectra for a sample of $[^{57}Fe_2^{III}Mn^{II}O(O_2CCH_3)_6(py)_3](py)$ doped into $[Mn_3O(O_2CCH_3)_6(py)_3](py)$. Error bars are contained within the size of the symbols.

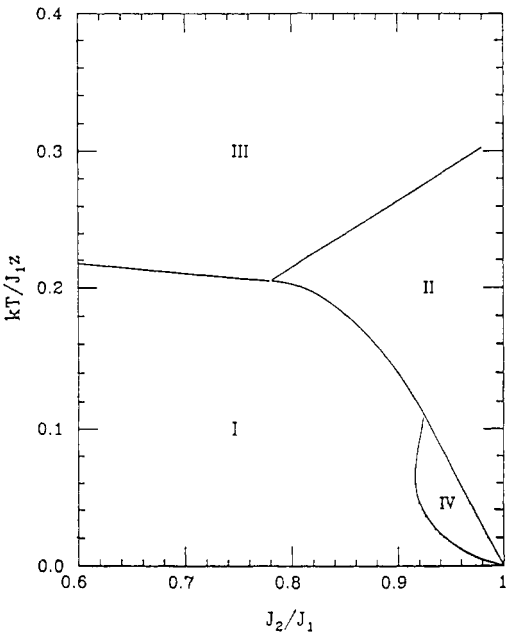

Figure 10. Phase diagram calculated by Stratt and Adachi[22] employing a mean field theory to account for the phase transitions in mixed-valence M_3O complexes, which crystallize in the *R*32 space group. The vertical axis is temperature plotted in units of J_1z/k, where k is the Boltzmann constant, z is the number of M_3O complexes surrounding each M_3O complex, and J_1 is the interaction energy of two neighboring complexes, both of which are distorted parallel to each other. The horizontal axis is the ratio of the antiferrodistortive (J_2) to the ferrodistortive (J_1) coupling, where J_2 is the interaction energy for two neighboring complexes, one of which is distorted and the other is undistorted.

Comments and Conclusions

$[Mn_3O(O_2CCH_3)_6(py)_3](py)$ exhibits a first-order phase transition at 184.65 K with a total entropy gain of $\Delta S = 35.77$ J K^{-1} mol^{-1} ($\simeq R$ ln 72). This is to be contrasted with $[Fe_3O(O_2CCH_3)_6(py)_3](py)$, which exhibits[11d] two transitions, a first-order one at ~ 112 K with $\Delta S = 4.61$ J K^{-1} mol^{-1} ($\simeq R$ ln 2) and a higher order phase transition, which starts at ~ 115 K and culminates at ~ 190 K with $\Delta S = 26.04$ J K^{-1} mol^{-1} ($\simeq R$ ln 22.9). The higher order phase transition was shown to involve both the conversion of the Fe_3O complex from valence trapped to valence detrapped and the onset of motion of the pyridine solvate molecule.

A possible explanation for why there is such a dramatic difference between the valence detrapping in the isostructural Fe_3O and Mn_3O complexes can be gleaned from recent theoretical papers.[21,22] Such a mixed-valence M_3O complex has a ground-

state potential energy surface that, depending on the levels of electronic and vibronic coupling, can have four minima. The pyridine–pyridine intermolecular interactions (Figure 1) have been treated by the molecular field approximation. Furthermore, Stratt and Adachi[22] took the insightful approach of employing a "spin"-type Hamiltonian, which leads logically to the idea of two interpenetrating sublattices of M_3O complexes. Figure 10 shows the phase diagram for these complexes. J_1 and J_2 are parameters that gauge the pairwise intermolecular interaction where two neighboring M_3O complexes are distorted parallel to each other or only one is distorted, respectively. At low temperatures, phase I (ferrodistortive phase) exists where all M_3O complexes are valence trapped, and because of strain dipoles, the sense of distortion of each M_3O complex is the same. In phase II (antiferrodistortive phase), two interpenetrating sublattices exist where one sublattice has valence-trapped complexes and the sense of distortion (i.e., which ion is the M^{II} ion) is random. The other sublattice has an appreciable number of undistorted (delocalized) complexes mixed with randomly oriented localized complexes. In phase III (paradistortive phase), there is random distribution of distorted and undistorted complexes, where each M_3O complex is probably tunneling rapidly between its four vibronic states. Phase IV is described as having two sublattices as in phase II, but with both sublattices "ferromagnetic" and distorted in the same direction. It is important to note that only the phase boundary between I–III, I–II, and IV–II phases gives first-order transitions. The other lines correspond to second-order transitions.

The differences in behavior between the present Mn_3O complex and the isostructural Fe_3O complex can be rationalized in terms of the phase diagram given in Figure 10. Previously, we explained the presence of two phase transitions in $[Fe_3O(O_2CCH_3)_6(py)_3](py)$ by saying that the first-order phase transition at ~112 K occurred between phases I and II. This is immediately followed by the onset of a higher order phase transition at ~115 K, which culminates at ~190 K at the phase II–III line. Because the Mn_3O complex has somewhat different a, b, and c unit cell parameters than the Fe_3O complex, the pyridine–pyridine intermolecular interactions are likely of different magnitude. The Mn_3O complex could have a J_2/J_1 ratio such that the only phase transition occurring is the first-order one between phases I and III. The Mn_3O complex converts directly between the ferrodistortive phase and the paradistortive phase without ever becoming the antiferrodistortive phase. Variable-temperature neutron diffraction experiments are planned in an effort to obtain direct evidence for the presence of interpenetrating sublattices of Mn_3O complexes.

Regardless of the detailed description of the phase present in $[Mn_3O(O_2CCH_3)_6(py)_3](py)$, it is amazing how cooperatively the valence detrapping occurs in this complex. There is long-range order as a result of appreciable intermolecular interactions. Not only are there appreciable intermolecular pyridine–pyridine interactions, but the interactions between Mn_3O complexes and pyridine solvate molecules are probably also important. It is clear that there is a sudden change from static to dynamic in the solvate structure at the 184.65 K phase transition. The two pyridine solvate molecules above and below each Mn_3O complex serve in essence as a small part of a solvate cage. The van der Waals interaction between a solvate molecule positioned asymmetrically relative to the C_3 axis of a nearby Mn_3O complex may lead to an intermolecular interaction energy of only 10–100 cm^{-1} per solvate molecule. This amount of energy may modify the ground-state potential energy surface of the Mn_3O complex and consequently appreciably affect the rate at which such a complex can tunnel from one vibronic minimum to another.

Acknowledgment. We are grateful for support from the National Institutes of Health Grant HL 13652 (D.N.H.), and National Science Foundation Grants DMB 8606358 (R.J.W.) and CHE-8507748 (G.C.).

(21) Kambara, T.; Hendrickson, D. N.; Sorai, M.; Oh, S. M. *J. Chem. Phys.* **1986**, *85*, 2895.
(22) Stratt, R. M.; Adachi, S. H. *J. Chem. Phys.* **1987**, *86*, 7156.

Determination of Stability Constants for Thallium(III) Cyanide Complexes in Aqueous Solution by Means of ^{13}C and ^{205}Tl NMR[1]

Johan Blixt, Bela Györi, and Julius Glaser*

Contribution from the Department of Inorganic Chemistry, The Royal Institute of Technology (KTH), S-100 44 Stockholm, Sweden. *Received February 10, 1989*

Abstract: In contrast to what is usually assumed, we have found and proved that thallium(III) forms very strong cyanide complexes in aqueous solution. We have investigated this system using ^{205}Tl, ^{13}C, and ^{14}N NMR and potentiometry and established the existence of four thallium(III)–cyanide complexes of the composition $Tl(CN)_n^{3-n}$, n = 1–4. We have measured their chemical shifts and spin–spin coupling constants and determined their formation constants at 25 °C in dilute (0.05 M) aqueous solution in the ionic medium ($[Na^+]$ = 1 M, $[Li^+]$ + $[H^+]$ = 3 M, $[ClO_4^-]$ = 4 M). The overall formation constants are log β_1 = 13.2 (1), log β_2 = 26.5 (2), log β_3 = 35.2 (2), and log β_4 = 42.6 (2). We have also determined the stability constant for HCN in the same ionic medium, log K_a = 10.11 (5). One-bond spin–spin coupling constants between thallium and carbon, $^1J(^{205}Tl–^{13}C)$, for the mono- and dicyano complexes of thallium(III) are 14636 and 13749 Hz, respectively, and appear to be the largest known coupling constants between these nuclei. The stability of the $Tl(CN)_n^{3-n}$ complexes is discussed in terms of their kinetic inertness.

The soft thallium(III) ion forms very strong complexes in solution. For example, its chloride and bromide complexes are among the strongest metal-ion halide complexes known. The soft cyanide ion, on the other hand, is a very important complexing ligand and forms strong complexes with most of the transition elements and the d^{10} ions. Also the Hg(II) ion, which is isoelectronic and has similar properties as Tl(III), forms very strong cyanide complexes.

* To whom correspondence should be addressed.

(1) Presented at the XIX International Conference on Solution Chemistry, Lund, Aug 1988. (cf. Abstracts, p 85).

0002-7863/89/1511-7784$01.50/0